Separation and Purification Technology 306 (2023) 122704

Contents lists available at ScienceDirect

Separation and Purification Technology

journal homepage: www.elsevier.com/locate/seppur

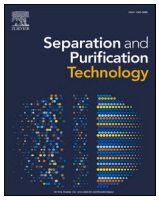

Room-temperature synthesis of ionic covalent organic frameworks for efficient removal of diclofenac sodium from aqueous solution

Hao-Ze Li [a,b,c], Cheng Yang [a,b,c], Hai-Long Qian [a,b,c], Xiu-Ping Yan [a,b,c,d,*]

[a] State Key Laboratory of Food Science and Technology, Jiangnan University, Wuxi 214122, China
[b] International Joint Laboratory on Food Safety, Jiangnan University, Wuxi 214122, China
[c] Institute of Analytical Food Safety, School of Food Science and Technology, Jiangnan University, Wuxi 214122, China
[d] Key Laboratory of Synthetic and Biological Colloids, Ministry of Education, Jiangnan University, Wuxi 214122, China

ARTICLE INFO

Keywords:
Room-temperature synthesis
Diclofenac sodium
Ionic covalent organic frameworks
Adsorption
Non-steroidal anti-inflammatory drugs

ABSTRACT

The excessive use of diclofenac sodium (DCF) has led to environmental and food safety problems. Effective removal of DCF in aqueous environment is of great significance. Ionic covalent organic frameworks (iCOFs) are effective adsorbents for the removal of pollutants due to their unique structure and properties, but conventional synthesis of iCOFs is limited by high temperature and long reaction time. Herein, we report a room-temperature strategy to synthesize iCOFs in 24 h for the first time. The room-temperature synthesized ionic COF (RT-iCOF) shows better crystallinity, lager uptake capacity and faster kinetics than those synthesized at high temperature with long reaction time. The adsorption kinetics, isotherms and thermodynamics, the effects of ionic strength, pH, humic acid, and reusability of RT-iCOF for DCF were studied in detail. The prepared RT-iCOF gave the maximum adsorption capacity of 857.5 mg g^{-1}, featuring the highest uptake capacity for DCF so far. The adsorption of DCF on the RT-iCOF are driven by ion exchange, π-π interactions, electrostatic and hydrogen bonds interaction. The adsorption efficiency of RT-iCOF for DCF was still above 90% after 5 regeneration cycles. This work also promotes the facile synthesis and application of iCOFs for the removal of pollutants.

1. Introduction

Diclofenac sodium (DCF), a widely prescribed nonsteroidal anti-inflammatory drug (NSAID), is frequently used for alleviating pain and anti-inflammatory [1]. However, the excessive use of DCF has led to widespread environmental contamination in many countries [2], and the most often detected NSAID in the environment [3]. The release of DCF led to harmful effects on resident species. At first, it was found that the death of vulture species resulted from the consumption of the DCF-treated carcasses of cattle [4]. Other studies also showed that DCF is harmful to aquatic organisms [5–7]. Moreover, DCF could bring about gastrointestinal damage, nephrotoxicity, hepatotoxicity, neurotoxicity, cardiotoxicity, genotoxicity in mammals even at a low concentration [8]. The polar, non-volatile and non-biodegradable properties of DCF make it difficult to remove and degrade [9,10]. Thus, it is urgent to explore an efficient method for removing DCF from aqueous environment.

Up to now, a number of approaches such as adsorption, biodegradation, membrane separation, advanced oxidation have been developed for DCF removal [11,12]. Among these strategies, adsorption has the advantages of simple operation, adequate availability, low cost and no byproducts [2,13]. Various adsorbents have been studied for DCF removal, such as zeolite [14,15], layered double hydroxides (LDHs) [16–18], resin [19] and activated carbon [20,21]. However, most of these materials exhibited slow adsorption kinetics and low capacity due to their uneven pores, and unstable structure [22]. Porous frameworks like metal–organic frameworks (MOFs) [23,24] and covalent organic frameworks (COFs) have been used in efficient removal of DCF [25–27].

Ionic covalent organic frameworks (iCOFs), which consist of ionic skeleton and corresponding counterions, are the subclass of COFs [28]. iCOFs have been applied in diverse fields such as conducting [29], catalysis [30], sensing [31] and adsorption [32–34]. The advantage of iCOFs in adsorption is that no post modification is required and the ionic sites on the skeleton provide homogeneous adsorption sites. Unlike neutral COFs, the existence of interlayer charge repulsion often leads to self-exfoliation or low-crystalline iCOFs [35,36], while higher crystalline iCOFs have been shown to give large adsorption capacity and fast adsorption kinetics [37]. Several methods were developed for rapid

* Corresponding author at: State Key Laboratory of Food Science and Technology, Jiangnan University, Wuxi 214122, China.
E-mail address: xpyan@jiangnan.edu.cn (X.-P. Yan).

https://doi.org/10.1016/j.seppur.2022.122704
Received 4 October 2022; Received in revised form 7 November 2022; Accepted 16 November 2022
Available online 17 November 2022

synthesis of high crystallinity neutral COFs at room temperature [38–41]. Although a few methods were reported to improve the crystallinity of iCOFs [37,42], high temperature (120 °C) along with a long reaction time (3 days) were still needed, which is unfavorable for the practical applications of iCOFs. Up to now, only one study on the removal of NSAID by iCOFs has been reported, in which, guanidine-based iCOFs were synthesized at 120 °C for 3 days. Although the guanidine-based iCOFs gave the adsorption capacity of 724.6 mg g^{-1} for DCF, the kinetics was slow (equilibrium time of 3 h) due to lower crystallinity [43]. Therefore, it is of great significance to explore iCOFs with easy synthesis, high crystallinity, high adsorption capacity, rapid kinetics and good recyclability.

Herein, we report room-temperature and fast synthesis of iCOF for the rapid removal of DCF for the first time. The adsorption performance of room-temperature synthesized iCOF (RT-iCOF) for DCF was evaluated in terms of adsorption kinetics thermodynamics and isotherms. The developed RT-iCOF showed a large adsorption capacity (857.5 mg g^{-1}) and rapid kinetics (equilibrium time of 30 min). The effects of inorganic ions, humic acid and pH on DCF removal were evaluated in details. The mechanism of DCF adsorption on RT-iCOF was explored by Fourier-transform infrared (FT-IR) spectra, X-ray photoelectron spectroscopy (XPS) and theoretical calculations. These results reveal enormous practical application potential of the RT-iCOF for the removal of DCF from water.

2. Materials and methods

2.1. Chemicals

All reagents used are at least of analytical grade. 1,3,5-triformylphloroglucinol (Tp) and 1,1′-bis(4-aminophenyl)-[4,4′-bipyridine]-1,1′-diium chloride (Vio-NH_2) were provided by Jilin Chinese Academy of Sciences-Yanshen Technology Co., ltd. (Jilin, China). Tetrahydrofuran (THF), methanol (MeOH), ethanol, acetonitrile (ACN), sodium hydroxide (NaOH), hydrochloric acid (HCl), formic acid, acetic acid (HAc) and all salts were purchased from Sinopharm Chemical Reagent Co. ltd. (Shanghai, China). Diclofenac sodium (DCF, 99%), Naproxen (NPX), Ketoprofen (KT), Acetylsalicylic acid (ASA), Ibuprofen (IBU), p-phenylenediamine (Pa-1), humic acid (HA), 1,2-dichlorobenzene (*o*-DCB), 1-butanol (*n*-BuOH), 1,4-dioxane and mesitylene were obtained from Aladdin Chemistry Co. ltd. (Shanghai, China). Ultrapure water was given by Wahaha Group Co. ltd. (Hangzhou, China). HPLC-grade ACN and MeOH were gotten from Fisher Chemical (Shanghai, China).

2.2. Synthesis of RT-iCOF

Tp (12.6 mg, 0.06 mmol) and Vio-NH_2 (37.2 mg, 0.09 mmol) were dispersed into an o-dichlorobenzene (*o*-DCB)/*n*-BuOH (1.4/0.6 mL) in a Schlenk tube (35 mL, o.d. = 26, length = 125 mm) via sonication. After addition of HAc (0.2 mL, 17.5 M), the mixture was further sonicated for 5 min and degassed under liquid N_2 (77 K) by three freeze–pump–thaw cycles. The tube was sealed and allowed to stand at room temperature for 24 h. The product was washed with THF and MeOH for several times. The powder collected was dried under vacuum at 60 °C overnight to yield brownish powder.

2.3. Instrumentation and characterization

Powder X-ray diffraction (PXRD) patterns were collected using a D2 PHASER diffractometer (Bruker AXS GmbH, Germany) equipped with a Cu K_α radiation with a scanning speed of 8° min^{-1} and a step size of 0.05° in 2θ. ^{13}C S NMR spectra were recorded on an ADVANCE III 400 MHz NMR (Bruker, Switzerland). Scanning electron microscopy (SEM) images were recorded on an a SU8100 SEM (Hitachi, Japan). The pore size and specific surface area were determined on Autosorb-iQ (Quantachrome, USA) using liquid nitrogen at 77 K. X-ray photoelectron spectroscopy (XPS) experiments were performed on Axis supra (Kratos, UK) and the binding energies were calibrated using the C1s peak at 284.8 eV. Fourier transform infrared (FT-IR) spectra were determined on Nicolet IR IS10 spectrometer (Nicolet, USA), and samples were prepared as KBr pellets.

2.4. Adsorption and regeneration experiments

For the adsorption isotherm study, 2 mg of RT-iCOF was added into 4 mL of DCF solution with different concentrations (200–1000 mg L^{-1}, initial pH 6.5). The suspensions were sonicated briefly and put in a controlled-temperature water bath with a rotating speed 150 of rpm. The adsorption was performed at 25, 35, 45 and 55 °C till equilibrium. Afterwards, the mixture was filtered on a syringe filter (0.22 μm), and the concentration of DCF in the filtrate was measured by HPLC.

For the kinetic experiment, RT-iCOF (10 mg) was added into 20 mL of DCF-containing solutions (200 and 400 mg L^{-1}). The mixture was sonicated briefly and put in a water bath (25 °C) with a rotating speed of 150 rpm. At a certain time (5, 10, 20, 30, 40, 50, 60, 90, 120, 180, 240, 300 min), 0.2 mL of the solutions were collected, filtered on syringe filter (0.22 μm), and analyezd by HPLC for DCF. The adsorption capacity (q, mg g^{-1}) was calculated using Eq. (1):

$$q = \frac{C_0 - C_t}{m} V \tag{1}$$

where C_0 (mg L^{-1}), C_t (mg L^{-1}), m (mg), and V (mL) correspond to the initial and final concentrations of DCF in solution, adsorbent mass, and solution volume, respectively.

To study the anti-disturbance ability of RT-iCOF, 1–20 mg L^{-1} humic acid, 0.01–100 mM anions (Cl^-, NO^{3-}, SO_4^{2-} and CO_3^{2-}) and cations (Na^+, K^+, Mg^{2+} and Ca^{2+}) were separately mixed with 500 mg L^{-1} DCF solutions. RT-iCOF (2 mg) was added in the 4 mL of mixed solutions with a rotating speed of 150 rpm at 25 °C until adsorption equilibrium. Furthermore, the effect of pH (6–11) was also tested.

The reusability of RT-iCOF was investigated as follows: 2 mg of RT-iCOF was added into 4 mL of DCF solution (100 mg L^{-1}) in a water bath (25 °C) with a rotating speed of 150 rpm to reach adsorption equilibrium. The pre-adsorbed material RT-iCOF-DCF was collected by centrifugation. The adsorbed DCF was then desorbed from RT-iCOF-DCF with 1 mL of MeOH for 5 min, while the solid adsorbent was collected by centrifugation. Desorption efficiency was determined by quantifying the concentration of DCF in desorption solution. The RT-iCOF was then regenerated by simply treating with 0.1 M HCl and applied for next adsorption–desorption cycle.

The concentration of DCF was measured using Waters alliance 2695 HPLC equipped with Waters XBridege® C18 column (5 μm, 4.6 mm × 250 mm) and 2998 PDA detector (Waters, U.S.A.) using ACN/0.1% aqueous formic acid solution (8:2, v/v) as the mobile phase at a flow rate of 1 mL min^{-1}. The column temperature was 25 °C. Chromatographic signals were monitored at 276 nm. All experiments were repeated independently-three times.

2.5. Adsorption location

In Materials Studio 2017, the low energy adsorption configuration of the DCF onto the accessible surface of the RT-iCOF was simulated using the Adsorption Locator modules with the COMPASSII forcefield [44]. The 6-layers slab contains 1 × 1 × 6 unit cells of AA-Eclipsed, 1 × 1 × 3 unit cells of AB-Staggered and 1 × 1 × 2 unit cells of ABC-Staggered were used for the adsorption simulation of DCF, respectively. The charges of the system were assigned using the COMPASSII forcefield. The maximum adsorption distance of 10 Å was selected. Metropolis Monte Carlo method was used to calculate the DCF adsorption on the RT-iCOF with with 10^5 Monte Carlo steps and 10 annealing cycles. The quality of the calculations for the optimization and adsorption processes was ultra-fine.

2.6. Application to real samples

To evaluate the practical removal applicability of RT-iCOF, blank samples (pure water, domestic water and lake) were used to prepare 10 mg L^{-1} DCF solutions. Removal experiments were conducted with the solid/liquid ratio of 0.2 g L^{-1} at 25 °C for 1 h.

3. Results and discussion

3.1. Synthesis and characterization of RT-iCOF

Tp and Vio-NH_2 were selected to synthesize stable iCOFs via an irreversible enol-to-keto tautomerization (Fig. 1a). To obtain high-crystallinity iCOFs, the effects of potential factors such as solvent, temperature, concentration of catalyst and reaction time were investigated in detail (Fig. S1-S5). The solubility of monomer varies with the composition and proportion of solvent, which in turn affects the reaction rate and thus the formation of high crystallinity iCOFs [45]. The combination of *o*-DCB/*n*-BuOH (7:3, v/v) was found to give a best crystallinity of iCOFs. High temperature is detrimental to the crystallinity of RT-iCOF, thus synthesis was conducted at room temperature. The best crystallinity of RT-iCOF was obtained in a reaction time of 24 h. As a result, the brownish powder RT-iCOF with the yield of *ca.* 48% was synthesized from Tp and Vio-NH_2 in the mixture of *o*-DCB/*n*-BuOH (1.4/0.6, v/v) with acetic acid (0.2 mL) at room temperature for 24 h.

To analyze the structure of RT-iCOF, PXRD and structural simulation experiments were conducted. The strong peak at 3.90° (1 1 0) identifies an ordered structure. Three other prominent peaks were observed at 7.80° (2 2 0), 12.38° (4 0 1) and 27.61° (4 1 3), in which the sharp peak at 27.61° suggest strong π-π stacking between the vertically stacked two-dimensional (2D) layers [35,36]. To elucidate the structure of RT-iCOF, several possible stacking 2D models (AA-eclipsed, AB-staggered and ABC-staggered) were built and optimized using Materials Studio (Fig. S6 – S7 and Fig. 1b – d). Obviously, the experimental PXRD pattern of RT-iCOF matches well with that simulated from the ABC staggered model (Fig. 2a). The Pawley refinement of ABC-staggered unit cell led to a space group of *R*-3 with a = b = 45.7649 ± 0.1037 Å, c = 10.5000 ± 0.0238 Å, α = β = 90° and γ = 120°, and the R_P and R_{WP} values of 1.56 and 2.26%, respectively (Fig. 2b and Table S1).

In the FT-IR spectrum of RT-iCOF, the disappearance of CH = O (2896 cm^{-1}) of Tp and N — H (3100–3300 cm^{-1}) of Vio-NH_2 indicates the total consumption of initial organic monomers (Fig. 2c). The ketone form was confirmed by the appearance of the peak at 1584 cm^{-1} of C═C and 1274 cm^{-1} of C — N. Fig. 2d shows the ^{13}C S NMR, the peak at 183 ppm arising from carbon of ketone further confirmed the formation of ketone form of RT-iCOF [46].

Fig. S8 shows the N_2 adsorption isotherms of RT-iCOF at 77 K. The Brunauer-Emmett-Teller (BET) surface area and total pore volume of the RT-iCOF were found to be 69 m^2 g^{-1} and 0.15 cm^3 g^{-1}, respectively (Fig. S9). The ABC staggered stacking of RT-iCOF resulted in relatively low specific surface area, for which another reason is the existence of Cl^- in the pore channels of RT-iCOF [22,35]. The pore-size distribution of RT-iCOF analyzed based on nonlocal density functional theory (NLDFT) is shown in Fig. S10. One prominent pore size distribution peak at 1.69 nm was also observed.

RT-iCOF was also characterized by SEM (Fig. S11). The chemical stability of RT-iCOF was tested in different reagents (Fig. S12). The good structural stability of RT-iCOF provides the foundation for the application in DCF removal in different environments.

3.2. Adsorption studies on RT-iCOF

The adsorption kinetics was investigated at two different concentrations (200 mg L^{-1} and 400 mg L^{-1}) at 25 °C. The adsorption was rapid at first 5 min (99% and 88% of removal efficiencies with the initial DCF concentrations of 200 and 400 mg L^{-1}, respectively), and then reached equilibrium in 30 min, which is one of the shortest equilibrium times for DCF adsorption among the reported adsorbents. Two kinetic models, pseudo-first-order (PFO) and pseudo-second-order (PSO) model, were further utilized to fit DCF adsorption kinetics. The kinetic studies revealed that the adsorption process was well-fitted by the PFO and PSO model ($R^2 \geq 0.99$, Table 1). However, the experimental equilibrium

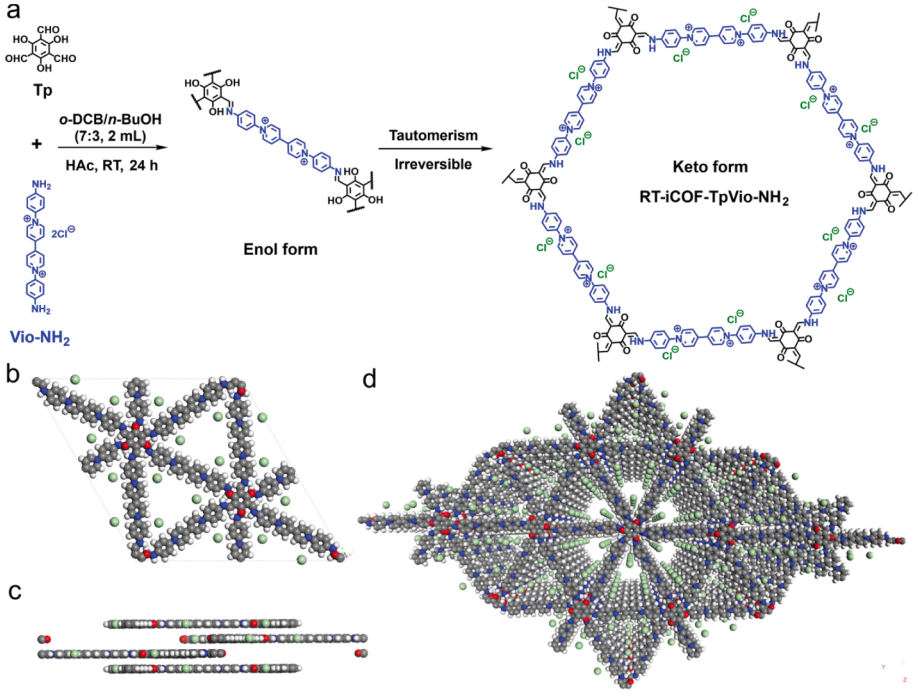

Fig. 1. (a) Synthetic scheme of RT-iCOF through the condensation of Tp and Vio-NH_2; (b) Unit cells of the ABC-staggered model of RT-iCOF; (c) side view of the ABC-staggered model of RT-iCOF; (d) Space-filling model of RT-iCOF in ABC-staggered model (gray, white, red, blue and green represent C, H, O, N, and Cl, respectively). (For interpretation of the references to colour in this figure legend, the reader is referred to the web version of this article.)

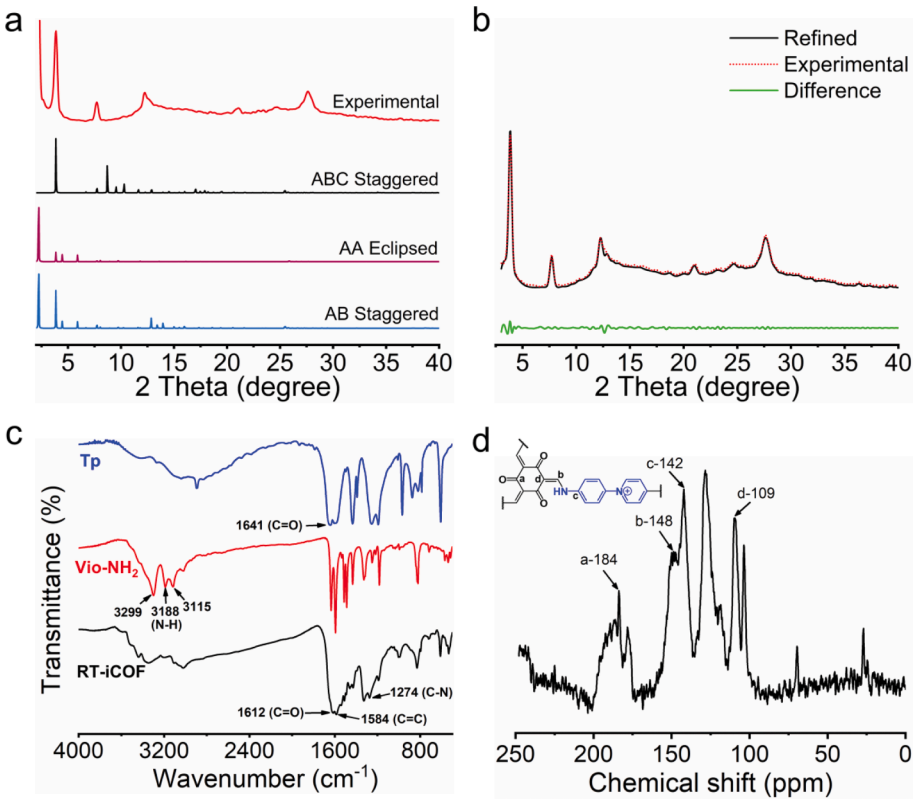

Fig. 2. (a) Experimental and simulated (AA, AB and ABC stacking model) PXRD patterns of RT-iCOF; (b) Pawley refinement of RT-iCOF (Rwp = 2.26%, Rp = 1.56%); (c) FT-IR spectra of Tp, Vio-NH_2 and RT-iCOF; (d) ^{13}C S NMR spectra of RT-iCOF.

Table 1
Adsorption kinetic parameters for DCF adsorption.

Models	Parameters	Initial concentrations	
		200 mg L^{-1}	400 mg L^{-1}
PSO	k_1 (min^{-1})	2.0746	0.6357
	q_e (mg g^{-1})	398.27	733.60
	R^2	0.9999	0.9982
PFO	k_2 (g mg^{-1} min^{-1})	0.0716	0.0050
	q_e (mgg^{-1})	398.86	740.54
	R^2	0.9995	0.9996
MO	k_1' (min^{-1})	0.1017	0.0237
	k_2' (g mg^{-1} min^{-1})	0.0635	0.0050
	R^2	0.9999	0.9975

adsorption capacities q_{exp} (398.7 and 743.3 mg g^{-1}) were close to those calculated by PSO model, and the PSO model gave the excellent linear fit to the experimental data (Fig. 3b). The practical adsorption process may be explained by both PFO and PSO models due to the complexity of adsorption kinetics process. Therefore, the mixed-order (MO) model was further used to identify the contribution to the adsorption with different kinetics models [27,47]. As shown in Table 1, the values of k_1' and k_2' obtained at different initial concentrations, confirm that the adsorption kinetics of DCF include PFO and PSO. Specifically, the contribution of PFO and PSO in the adsorption process is presented in Fig. 3c, d. At the initial stage of adsorption, the PSO rate was much higher than that of PFO rate, later the PFO rate is slightly higher until the adsorption equilibrium at the rate of zero. Moreover, the PSO rate was much higher than the PFO rate, and the values of k_2' were close to k_2, indicating that PSO played a leading role in the adsorption kinetics. Thus, the adsorption process of RT-iCOF for DCF was dominated by chemical adsorption [48].

The adsorption isotherms were analyzed with the initial DCF concentrations of 200–1000 mg L^{-1} at 25–55 °C. Fig. 3e shows the fitting curves of the Langmuir and Freundlich model, and the adsorption parameters are displayed in Table 2. The Langmuir model fitted adsorption data better than Freundlich model ($0.9717 < R^2 < 0.9947$ for Langmuir and $0.7068 < R^2 < 0.8591$ for Freundlich). Fig. 2f shows the linear fitting of Langmuir model. Moreover, q_m values calculated from Langmuir model are similar to those of experimental q_{exp}, indicating DCF adsorption onto RT-iCOF is monolayer with a limited adsorption sites [49]. The experimental and theoretical maximum sorption capacity of diclofenac with RT-iCOF were 875.0 and 857.5 mg g^{-1}, respectively (Table 2), which is the highest sorption capacity among the reported adsorbents for DCF removal (Table S2). Similar adsorption capacity (862.0 mg g^{-1}) was also obtained with a larger amount of RT-iCOF (50 mg in 100 mL DCF solution). The separation factor or equilibrium parameter (R_L), which can be used to determines if the adsorption is favourable ($0 < R_L < 1$) or unfavourable ($R_L > 1$) [50], was also calculated (Eq. S7). The values of R_L were in the range of 0.0016–0.0286, indicating a favorable adsorption of DCF by RT-iCOF. Although the Freundlich shows a poor fit, the intensity factor $1/n$ can give the information about the ease of adsorption. The values of $1/n$ in the range of 0.094–0.114 indicate the highly favorable adsorption [51]. The distribution coefficient value (K_d) is a measure of sorbent's affinity for targets, and a sorbent with a K_d value above 1.0×10^5 mL g^{-1} is usually considered excellent [52]. The calculated K_d value of RT-iCOF's affinity for DCF is 2.96×10^5 mL g^{-1} (Eq. S8), which is 10 times and 20 times higher than that of iCOF-TPA-TG_{Cl} (2.8×10^4 mL g^{-1}) [43] and LDH-PmPD (1.3×10^4 mL g^{-1}) [18], respectively.

The adsorption thermodynamics studies were conducted at different temperatures (Fig. 3e). The obtained parameters Gibbs energy (ΔG°), enthalpy (ΔH°) and entropy (ΔS°) can be used to understand adsorption feasibility and mechanism. The calculated thermodynamic parameters are presented in Fig. S13 and Table S3. The negative values of ΔG° at different temperatures confirm that the adsorption of DCF by RT-iCOF is a spontaneous process [50]. The negative value of ΔH° endorses the

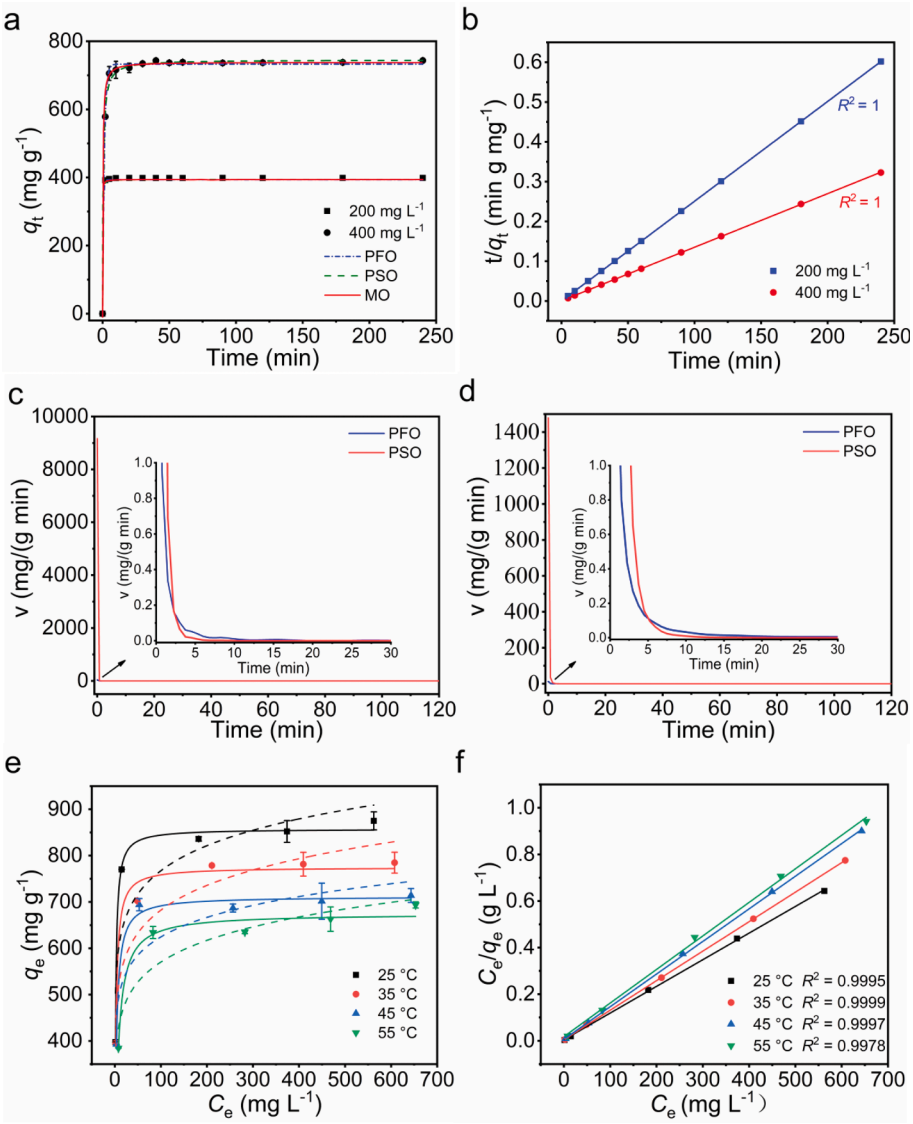

Fig. 3. (a) Adsorption kinetics of RT-iCOF for DCF (10 mg of RT-iCOF in 20 mL of 200 and 400 mg L^{-1} DCF solutions); (b) PSO kinetics adsorption linear fitting plots of DCF with different initial concentrations; (c) and (d) Contribution of the PFO rate and the PSO rate in adsorption process; (e) Adsorption isotherms of RT-iCOF for DCF from 25 °C to 55 °C, solid line for Langmuir model and dashed line for Freundlich model (2 mg of RT-iCOF in 4 mL of 200–1000 mg L^{-1} DCF solutions); (f) Fitting plots of adsorption isotherms of DCF on RT-iCOF Langmuir model.

Table 2
Parameters of adsorption isotherm models for DCF adsorption.

Models	Parameters	Temperatures (K)			
		298.15	308.15	318.15	328.15
Langmuir	q_{exp} (mg g^{-1})	875.0 ± 19.4	784.7 ± 22.5	713.9 ± 14.9	693.7 ± 6.7
	q_m (mg g^{-1})	857.5 ± 7.9	774.7 ± 13.6	711.7 ± 8.3	674.7 ± 11.6
	K_L (L mg^{-1})	0.63	0.46	0.34	0.17
	$R_L \times 10^2$	0.16 – 0.79	0.22 – 1.08	0.29 – 1.45	0.58 – 2.86
	R^2	0.9947	0.9762	0.9872	0.9717
Freundlich	K_F (L mg^{-1})	488.7 ± 10.2	413.9 ± 57.3	405.0 ± 73.1	338.1 ± 54.4
	n	10.2 ± 3.4	9.2 ± 2.2	10.6 ± 3.8	8.8 ± 2.2
	$1/n$	0.098	0.109	0.094	0.114
	R^2	0.7381	0.8591	0.7068	0.8278

exothermic nature of sorption process [53], which is consistent with the experimental phenomenon that the adsorption capacity decreases with the increase of temperature. The negative value of ΔS° confirms the decrease of the freedom degree of the adsorption process [54].

3.3. Effect of inorganic ions, humic acid and pH on DCF adsorption

The exsistance of various inorganic ions and molecules in real water samples may effect, the adsorption of DCF on RT-iCOF may be affected. Therefore, the effects of the species and concentration of inorganic ions, the concentration of humic acid and pH were studied in detail. The presence of cations had slight negative effect on adsorption capacity (except for Mg^{2+}) (Fig. 4a). This phenomenon can be attributed to the cation-mediated shielding effect, while cations also enhanced electrostatic effect, especially divalent cation Mg^{2+} [55,56]. In general, the presence of cations has no significant negative effect on the removal of DCF. The presence of anions can decrease the adsorption capacity of RT-iCOF, and this phenomenon is more pronounced for divalent anions than monovalent anions (Fig. 4b), the stronger competitive adsorption by bivalent anions than monovalent anions. The increase of adsorption capacity at a few concentrations may be due to the salting-out effect [57]. In additon, the effect of anion on adsoprtion decreased in order of $CO_3^{2-} > SO_4^{2-} > Cl^- > NO_3^-$, which is consistent with their standard Gibbs energies of hydration $\triangle G_h^\circ$ − 1315, − 1090, − 347 and − 306 kJ mol^{-1}, respectively [58]. This phenomenon follows the non-Hofmeister bias because of the hydrophobic skeleton of RT-iCOF [59]. Furthermore, the anion with lager radius are softer bases with greater affinity towards soft acid viologen sites of RT-iCOF, so the softer SO_4^{2-} ($r = 0.218$ nm) and

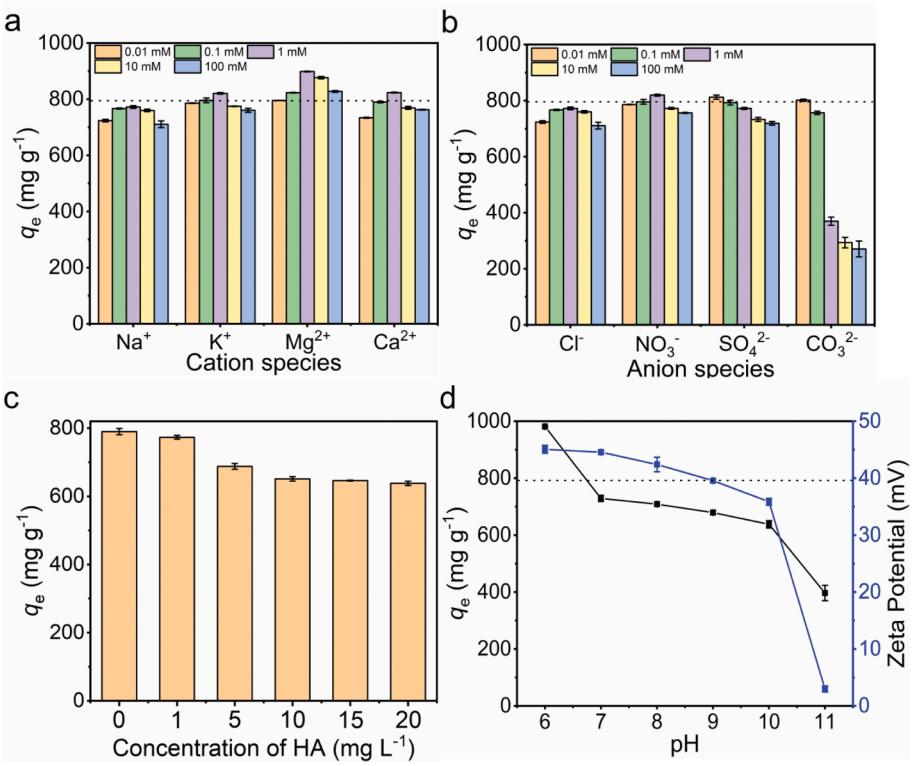

Fig. 4. (a) Effect of cations species and concentrations; (b) Effect of anions species and concentrations; (c) Effect of humic acid; (d) Effect of pH and zeta potential of RT-iCOF. In all cases, the concentration of DCF is 500 mg L^{-1} with pH = 6.5, solid/liquid = 2 mg/4mL, 25 °C, time = 1 h. Dashed lines represent control.

CO_3^{2-} (r = 0.189 nm) offers favorably binding to RT-iCOF than Cl^- (r = 0.181 nm).

The effect of HA was studied in the concentration of 1–20 mg L^{-1}. With the increase of humic acid concentration, the adsorption capacity of DCF on RT-iCOF decreased from 790 to 648 mg g^{-1} (Fig. 4c). The zeta potential of HA is negative at pH > 1.5, originating from the deprotonation carboxylic and phenolic groups [60]. Therefore, the adsorption sites on RT-iCOF were partially occupied by negatively charged HA, leading to the decrease of adsorption capacity.

The effect of pH on DCF adsorption and zeta potential of RT-iCOF is shown in Fig. 4d. The solubility of DCF (pK_a 4.2) was low at pH < pK_a [43], so the adsorption behavior of RT-iCOF for DCF was studied at pH 6–11. pH 6 gave the q_e of 981 mg g^{-1} due to the precipitation from the reduced solubility of DCF. The value of q_e decreased slowly with an increase in pH and decreased sharply at pH 11, in good agreement with the pH dependence of zeta potential of RT-iCOF (Fig. 4d). The zeta potential of RT-iCOF is all positive (Fig. 4d), while DCF dissociates into anion forms in the pH range studied. The viologen cation sites were deprotonated with pH increasing, resulting in weakening the interaction between RT-iCOF and DCF. However, a certain degree of adsorption occurred even under strong alkali environment likely due to the π-π interaction and hydrogen bonding, The detailed proof will be developed in the following sections.

3.4. Cycle adsorption performance

Optimization of desorption solvent (ethanol, acetonitrile, methanol and 0.1 M NaOH), desorption volume (0.5–3 mL) and desorption time (2–30 min) led to a desorption efficiency of 91% with 1 mL of methanol for 5 min desorption (Fig. S14). The desorbed RT-iCOF was transformed into a cationic form by 0.1 M HCl for 1 h [32]. After five cycles of adsorption–desorption, RT-iCOF still gave over 90% removal efficiency for DCF (Fig. S15), and the PXRD pattern of regenerated RT-iCOF indicated the decrease of crystallinity (Fig. S16).

3.5. Adsorption mechanism

To further explore the reasons for the high adsorption capacity and fast kinetics of RT-iCOF, TpPa-1 [46], which has similar structure and pore size of RT-iCOF but contains no viologen cation, was prepared for comparison (Fig. S17). TpPa-1 merely gave low capacity of 20 mg g^{-1} for DCF (Fig. S18) owing to the high polarity of DCF, demonstrating the dominant role of the viologen cation of RT-iCOF in adsorption. Furthermore, the iCOF was also synthesized at 120 °C for 6 days [36], and lower crystallinity SCU-COF-1 was obtained (Fig. S19). Compared with RT-iCOF, the adsorption capacity of SCU-COF-1 was reduced by 20%, and the equilibrium time greatly increased (about 3 h) (Fig. S20). This can be ascribed to more ordered channels and more adsorption sites exposed in the higher crystalline RT-iCOF [37].

The interaction between RT-iCOF and DCF was evaluated by XPS (Fig. 5, S21 and S22). Fig. 5a shows that the characteristic peaks of C 1 s for C═O (289.10 eV) and C—N (286.26 eV) of RT-iCOF slightly changed after DCF loading (289.00 eV for C═O and 286.02 for C—N) [61]. As shown in Fig. 5b, the binding energy of N 1 s for viologen = N^+– and amine –NH– was shifted from 402.13 and 400.17 eV to 402.46 and 399.95 eV, respectively [62], demonstrating the interaction of viologen = N^+– and DCF. The N 1 s relative peak area for –NH– significantly increased due to the contribution of adsorbed DCF. The O 1 s spectra of RT-iCOF was assigned to protonated C = OH^+ (532.61 eV) and C═O (530.85 eV) [33,53]. After the adsorption, the O 1 s peak of C = OH^+ shifted to 532.05 eV, and a new O 1 s peak at 533.24 eV associated with –COO^- of DCF appeared (Fig. 5c) [56]. Moreover, the decrease in the O 1 s peak area of C = OH^+ in company with an increase in the O 1 s peak area of C═O might result from the interaction between protonated C = OH^+ and –COO^- of DCF [63]. The Cl 2p spectrum of RT-iCOF was ascribed to Cl^- $2p_{1/2}$ and Cl^- $2p_{3/2}$ at 198.26 and 196.89 eV, respectively [64]. After uptake of DCF, free Cl^- was not observed and two peaks at 202.69 eV ($2p_{3/2}$) and 200.69 eV ($2p_{1/2}$) for the C-Cl of DCF appeared (Fig. 5d). In addition, sodium was not detected before and

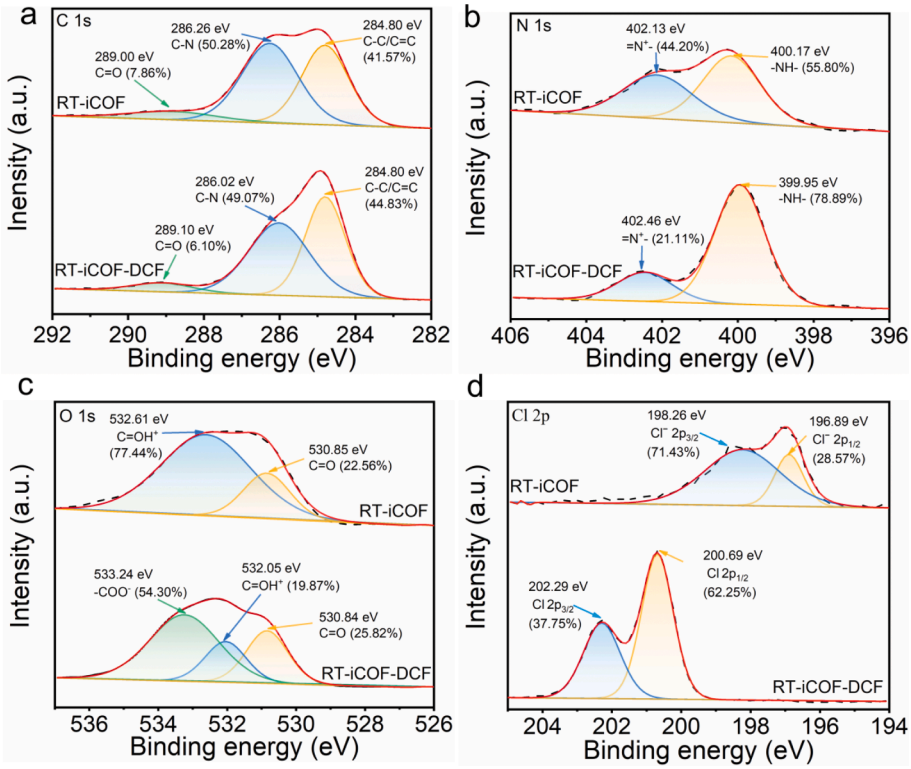

Fig. 5. Deconvolution analysis of C 1 s (a), N 1 s (b), O 1 s (c) and Cl 2p (d) XPS spectra of fresh RT-iCOF and RT-iCOF-DCF (dashed lines and red lines represent raw curves and fitting curves, respectively). (For interpretation of the references to colour in this figure legend, the reader is referred to the web version of this article.)

after adsorption. These results can be attributed to the exchange of hard base Cl^- with soft base DCF anion in conjugation with the formation of hard base (Cl^-)-hard acid (Na^+) and soft base (DCF^-)-soft acid ion (viologen = N^+–) pairs [65]. To further prove the occurrence of ion exchange, the Cl 2p XPS spectra of the HCl-regenerated RT-iCOF after MeOH elution were measured (Fig. S22). After desorption, the Cl 2p peaks for the C-Cl of DCF disappeared while the Cl 2p intensity for the Cl^- of RT-iCOF decreased to extremely low levels. HCl treatment made the Cl 2p intensity of Cl^- return to a level equivalent to that of the original RT-iCOF. The above results confirm the occurrence of ion exchange and the full regeneration of RT-iCOF with HCl.

The FT-IR spectra of RT-iCOF before and after the adsorption of DCF are shown in Fig. 6. The phenyl C═C stretching of RT-iCOF at 1584 cm^{-1}, the phenyl C═C stretching at 1574 cm^{-1} and C – Cl stretching at 746 cm^{-1} of DCF changed after adsorption as the result of the π-π interaction between DCF and RT-iCOF [61]. After the adsorption of DCF,

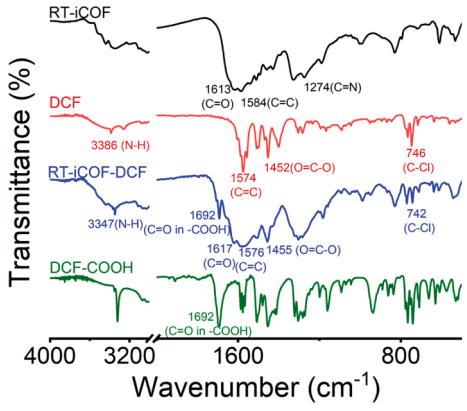

Fig. 6. FT-IR spectra of RT-iCOF, DCF and DCF adsorbed RT-iCOF (RT-iCOF-DCF) and DCF-COOH.

the N — H stretching at 3386 cm^{-1}, the O═C-O stretching at 1452 cm^{-1} of DCF and the C═O stretching of RT-iCOF at 1613 cm^{-1} shifted to 3347 cm^{-1}, 1455 cm^{-1} and 1617 cm^{-1}, respectively [18], due to the hydrogen-bond interaction. A new band at 1692 cm^{-1} of RT-iCOF-DCF can be attributed to the C═O stretching of – COOH [24]. The same band was also observed in diclofenac acid (DCF-COOH), which again confirmed the ion exchange in adsorption process. In addition, the FT-IR spectra of the regenerated RT-iCOF show no obvious difference (Fig. S23).

The lowest energy adsorption configurations of DCF adsorbed on the different stacking modes of RT-iCOF are presented in Fig. 7. Because the above experimental results proved the ion exchange mechanism for the adsorption, the Cl^- of RT-iCOF and Na^+ of DCF were left out in Adsorption Location here. The adsorption of DCF all occurred inside the channel structure of RT-iCOF, and the carboxyl groups of DCF were directed towards the viologen groups, confirming the adsorption site of viologen. In the AA-eclipsed, benzene ring structure of DCF was nearly vertical to that of RT-iCOF whereas the H-bonding interaction was not observed. A similar situation was also observed in a previous study [27]. In two staggered stacking modes, the DCF molecules were accommodated between the layers of RT-iCOF after adsorption, and the benzene ring structure of DCF was nearly parallel to that of RT-iCOF, indicating the existence of π-π stacking interaction. Although hydrogen bonding was also not observed in AB staggered mode, the N—H···O═C H-bonding interaction was seen in ABC-staggered mode. This can be attributed to more adsorption sites exposed in more staggered structures. The calculated adsorption energy of DCF on RT-iCOF was – 47.14 kcal mol^{-1}, indicating that the adsorption process was exothermic and the geometrical structure of RT-iCOF-DCF stable [34].

In summary, the adsorption process is driven by a variety of interactions, among which electrostatic interaction in company with ion exchange is the main driving force while π-π interaction and hydrogen bonding also participate in the adsorption process.

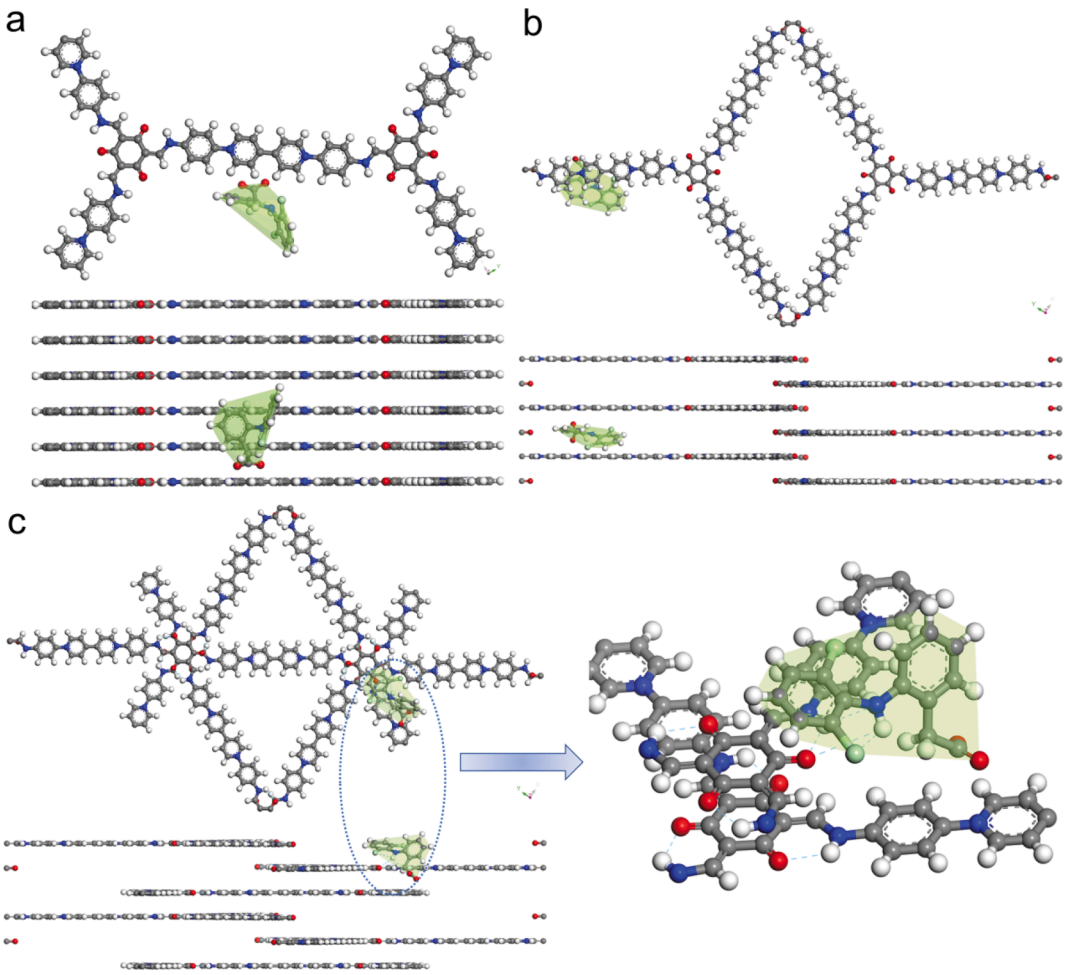

Fig. 7. Lowest energy adsorption configuration of DCF adsorbed on different stacking modes of RT-iCOFs. (a) AA-eclipsed; (b) AB-staggered and (c) ABC-staggered.

3.6. Removal of DCF in real water samples

The applicability of RT-iCOF in real environmental water samples was examined. As illustrated in Fig. S24, the removal efficiencies were 99.9%, 99.5% and 97.6% in pure water, domestic water and lake water with the DCF concentration of 10 mg L^{-1}, respectively. The complexity of environmental water samples only made a slight reduction in removal efficiency. In addition, the removal efficiency of DCF remained 91.8% in the mixed aqueous solution of five NSAIDs, which was significantly higher than that of other NSAIDs (Fig. S25). The good performance of RT-iCOF shows its feasibility for practical application in DCF water treatment.

4. Conclusion

We have first reported a strategy for the synthesis of iCOF at room temperature for 24 h. The synthesized RT-iCOF is an excellent adsorbent for DCF with fast kinetics, large adsorption capacity, good stability and recyclability. The adsorption is dominated by chemical adsorption with spontaneous exothermic process. DCF is adsorbed on RT-iCOF by ion exchange, electrostatic, π-π and hydrogen bonding interaction. Overall, the developed RT-iCOF with facile fabrication and excellent adsorption performance has a great potential for DCF removal in practical water treatments.

CRediT authorship contribution statement

Hao-Ze Li: Conceptualization, Investigation, Data curation, Validation, Writing – original draft. **Cheng Yang:** Validation. **Hai-Long Qian:** Validation. **Xiu-Ping Yan:** Conceptualization, Project administration, Writing – review & editing, Funding acquisition, Supervision.

Declaration of Competing Interest

The authors declare that they have no known competing financial interests or personal relationships that could have appeared to influence the work reported in this paper.

Data availability

Data will be made available on request.

Acknowledgements

This work was supported by the National Natural Science Foundation of China (22176073 and 22076066), the Fundamental Research Funds for the Central Universities (No. JUSRP221002), the Program of "Collaborative Innovation Center of Food Safety and Quality Control in Jiangsu Province".

Appendix A. Supplementary material

Supplementary data to this article can be found online at https://doi.org/10.1016/j.seppur.2022.122704.

References

[1] S. Zhang, X. Qu, H. Tang, Y. Wang, H. Yang, W. Yuan, B. Yue, Diclofenac Resensitizes Methicillin-Resistant Staphylococcus aureus to beta-Lactams and Prevents Implant Infections, Adv. Sci. 8 (2021) 2100681, https://doi.org/10.1002/advs.202100681.

[2] M. Patel, R. Kumar, K. Kishor, T. Mlsna, C.U. Pittman Jr., D. Mohan, Pharmaceuticals of Emerging Concern in Aquatic Systems: Chemistry, Occurrence, Effects, and Removal Methods, Chem. Rev. 119 (2019) 3510–3673, https://doi.org/10.1021/acs.chemrev.8b00299.

[3] B.S. He, J. Wang, J. Liu, X.M. Hu, Eco-pharmacovigilance of non-steroidal anti-inflammatory drugs: Necessity and opportunities, Chemosphere 181 (2017) 178–189, https://doi.org/10.1016/j.chemosphere.2017.04.084.

[4] B. Bonnefille, E. Gomez, F. Courant, A. Escande, H. Fenet, Diclofenac in the marine environment: A review of its occurrence and effects, Mar. Pollut. Bull. 131 (2018) 496–506, https://doi.org/10.1016/j.marpolbul.2018.04.053.

[5] M.N. Ajima, O.A. Ogo, B.S. Audu, K.C. Ugwoegbu, Chronic diclofenac (DCF) exposure alters both enzymatic and haematological profile of African catfish, Clarias gariepinus, Drug Chem. Toxicol. 38 (2015) 383–390, https://doi.org/10.3109/01480545.2014.974108.

[6] Q. Fu, D. Fedrizzi, V. Kosfeld, C. Schlechtriem, V. Ganz, S. Derrer, D. Rentsch, J. Hollender, Biotransformation Changes Bioaccumulation and Toxicity of Diclofenac in Aquatic Organisms, Environ. Sci. Technol. 54 (2020) 4400–4408, https://doi.org/10.1021/acs.est.9b07127.

[7] H. Zind, L. Mondamert, Q.B. Remaury, A. Cleon, N.K.V. Leitner, J. Labanowski, Occurrence of carbamazepine, diclofenac, and their related metabolites and transformation products in a French aquatic environment and preliminary risk assessment, Water Res. 196 (2021), 117052, https://doi.org/10.1016/j.watres.2021.117052.

[8] P. Sathishkumar, K. Mohan, R.A.A. Meena, M. Balasubramanian, L. Chitra, A. R. Ganesan, T. Palvannan, S.K. Brar, F.L. Gu, Hazardous impact of diclofenac on mammalian system: Mitigation strategy through green remediation approach, J. Hazard. Mater. 419 (2021), 126135, https://doi.org/10.1016/j.jhazmat.2021.126135.

[9] R. Loos, R. Carvalho, D.C. Antonio, S. Comero, G. Locoro, S. Tavazzi, B. Paracchini, M. Ghiani, T. Lettieri, L. Blaha, B. Jarosova, S. Voorspoels, K. Servaes, P. Haglund, J. Fick, R.H. Lindberg, D. Schwesig, B.M. Gawlik, EU-wide monitoring survey on emerging polar organic contaminants in wastewater treatment plant effluents, Water Res. 47 (2013) 6475–6487, https://doi.org/10.1016/j.watres.2013.08.024.

[10] L. Lonappan, S.K. Brar, R.K. Das, M. Verma, R.Y. Surampalli, Diclofenac and its transformation products: Environmental occurrence and toxicity - A review, Environ. Int. 96 (2016) 127–138, https://doi.org/10.1016/j.envint.2016.09.014.

[11] I. Alessandretti, C.V.T. Rigueto, M.T. Nazari, M. Rosseto, A. Dettmer, Removal of diclofenac from wastewater: A comprehensive review of detection, characteristics and tertiary treatment techniques, J. Environ. Chem. Eng. 9 (2021), https://doi.org/10.1016/j.jece.2021.106743.

[12] O.M. Rodriguez-Narvaez, J.M. Peralta-Hernandez, A. Goonetilleke, E.R. Bandala, Treatment technologies for emerging contaminants in water: A review, Chem. Eng. J. 323 (2017) 361–380, https://doi.org/10.1016/j.cej.2017.04.106.

[13] S. Zhuang, R. Cheng, J. Wang, Adsorption of diclofenac from aqueous solution using UiO-66-type metal-organic frameworks, Chem. Eng. J. 359 (2019) 354–362, https://doi.org/10.1016/j.cej.2018.11.150.

[14] K. Sun, Y. Shi, X. Wang, Z. Li, Sorption and retention of diclofenac on zeolite in the presence of cationic surfactant, J. Hazard. Mater. 323 (2017) 584–592, https://doi.org/10.1016/j.jhazmat.2016.08.026.

[15] D. Smiljanić, B. de Gennaro, F. Izzo, A. Langella, A. Daković, C. Germinario, G. E. Rottinghaus, M. Spasojević, M. Mercurio, Removal of emerging contaminants from water by zeolite-rich composites: A first approach aiming at diclofenac and ketoprofen, Microporous Mesoporous Mater. 298 (2020), 110057, https://doi.org/10.1016/j.micromeso.2020.110057.

[16] H. Xu, S. Zhu, M. Xia, F. Wang, Rapid and efficient removal of diclofenac sodium from aqueous solution via ternary core-shell CS@PANI@LDH composite: Experimental and adsorption mechanism study, J. Hazard. Mater. 402 (2021), 123815, https://doi.org/10.1016/j.jhazmat.2020.123815.

[17] H. Mkaddem, E. Rosales, M. Pazos, H. Ben Amor, M.A. Sanromán, J. Meijide, Anti-inflammatory drug diclofenac removal by a synthesized MgAl layered double hydroxide, J. Mol. Liq. 359 (2022), 119207, https://doi.org/10.1016/j.molliq.2022.119207.

[18] T. Xiong, X. Yuan, H. Wang, Z. Wu, L. Jiang, L. Leng, K. Xi, X. Cao, G. Zeng, Highly efficient removal of diclofenac sodium from medical wastewater by Mg/Al layered double hydroxide-poly(m-phenylenediamine) composite, Chem. Eng. J. 366 (2019) 83–91, https://doi.org/10.1016/j.cej.2019.02.069.

[19] X. Lu, Y. Shao, N. Gao, J. Chen, Y. Zhang, Q. Wang, Y. Lu, Adsorption and removal of clofibric acid and diclofenac from water with MIEX resin, Chemosphere 161 (2016) 400–411, https://doi.org/10.1016/j.chemosphere.2016.07.025.

[20] P.V. Viotti, W.M. Moreira, O.A.A.d. Santos, R. Bergamasco, A.M.S. Vieira, M. F. Vieira, Diclofenac removal from water by adsorption on Moringa oleifera pods and activated carbon: Mechanism, kinetic and equilibrium study, J. Clean. Prod. 219 (2019) 809–817, https://doi.org/10.1016/j.jclepro.2019.02.129.

[21] B.N. Bhadra, P.W. Seo, S.H. Jhung, Adsorption of diclofenac sodium from water using oxidized activated carbon, Chem. Eng. J. 301 (2016) 27–34, https://doi.org/10.1016/j.cej.2016.04.143.

[22] H.J. Da, C.X. Yang, X.P. Yan, Cationic Covalent Organic Nanosheets for Rapid and Selective Capture of Perrhenate: An Analogue of Radioactive Pertechnetate from Aqueous Solution, Environ. Sci. Technol. 53 (2019) 5212–5220, https://doi.org/10.1021/acs.est.8b06244.

[23] S. Zhuang, Y. Liu, J. Wang, Mechanistic insight into the adsorption of diclofenac by MIL-100: Experiments and theoretical calculations, Environ. Pollut. 253 (2019) 616–624, https://doi.org/10.1016/j.envpol.2019.07.069.

[24] H.A. Younes, M. Taha, R. Mahmoud, H.M. Mahmoud, R.M. Abdelhameed, High adsorption of sodium diclofenac on post-synthetic modified zirconium-based metal-organic frameworks: Experimental and theoretical studies, J. Colloid Interface Sci. 607 (2022) 334–346, https://doi.org/10.1016/j.jcis.2021.08.158.

[25] J. Hao, Q. Zhang, P. Chen, X. Zheng, Y. Wu, D. Ma, D. Wei, H. Liu, G. Liu, W. Lv, Removal of pharmaceuticals and personal care products (PPCPs) from water and wastewater using novel sulfonic acid (–SO3H) functionalized covalent organic frameworks, Environ. Sci, NANO 6 (2019) 3374–3387, https://doi.org/10.1039/c9en00708c.

[26] J.-B. Feng, Y.-Y. Li, Y. Zhang, Y.-Y. Xu, X.-W. Cheng, Adsorptive removal of indomethacin and diclofenac from water by polypyrrole doped-GO/COF-300 nanocomposites, Chem. Eng. J. 429 (2022), 132499, https://doi.org/10.1016/j.cej.2021.132499.

[27] S. Zhuang, R. Chen, Y. Liu, J. Wang, Magnetic COFs for the adsorptive removal of diclofenac and sulfamethazine from aqueous solution: Adsorption kinetics, isotherms study and DFT calculation, J. Hazard. Mater. 385 (2020), 121596, https://doi.org/10.1016/j.jhazmat.2019.121596.

[28] P. Zhang, Z. Wang, P. Cheng, Y. Chen, Z. Zhang, Design and application of ionic covalent organic frameworks, Coord. Chem. Rev. 438 (2021), 213873, https://doi.org/10.1016/j.ccr.2021.213873.

[29] Y. Peng, G. Xu, Z. Hu, Y. Cheng, C. Chi, D. Yuan, H. Cheng, D. Zhao, Mechanoassisted Synthesis of Sulfonated Covalent Organic Frameworks with High Intrinsic Proton Conductivity, ACS Appl. Mater. Interfaces 8 (2016) 18505–18512, https://doi.org/10.1021/acsami.6b06189.

[30] L.-G. Ding, B.-J. Yao, F. Li, S.-C. Shi, N. Huang, H.-B. Yin, Q. Guan, Y.-B. Dong, Ionic liquid-decorated COF and its covalent composite aerogel for selective CO2 adsorption and catalytic conversion, J. Mater. Chem. A 7 (2019) 4689–4698, https://doi.org/10.1039/c8ta12046c.

[31] A. Mal, R.K. Mishra, V.K. Praveen, M.A. Khayum, R. Banerjee, A. Ajayaghosh, Supramolecular Reassembly of Self-Exfoliated Ionic Covalent Organic Nanosheets for Label-Free Detection of Double-Stranded DNA, Angew. Chem. Int. Ed. 57 (2018) 8443–8447, https://doi.org/10.1002/anie.201801352.

[32] S. Jansone-Popova, A. Moinel, J.A. Schott, S.M. Mahurin, I. Popovs, G.M. Veith, B. A. Moyer, Guanidinium-Based Ionic Covalent Organic Framework for Rapid and Selective Removal of Toxic Cr(VI) Oxoanions from Water, Environ. Sci. Technol. 53 (2019) 878–883, https://doi.org/10.1021/acs.est.8b04215.

[33] X. Zhuang, J. Hao, X. Zheng, D. Fu, P. Mo, Y. Jin, P. Chen, H. Liu, G. Liu, W. Lv, High-performance adsorption of chromate by hydrazone-linked guanidinium-based ionic covalent organic frameworks: Selective ion exchange, Sep. Purif. Technol. 274 (2021), 118993, https://doi.org/10.1016/j.seppur.2021.118993.

[34] W. Wang, Z. Zhou, H. Shao, S. Zhou, G. Yu, S. Deng, Cationic covalent organic framework for efficient removal of PFOA substitutes from aqueous solution, Chem. Eng. J. 412 (2020), 127509, https://doi.org/10.1016/j.cej.2020.127509.

[35] H. Chen, H. Tu, C. Hu, Y. Liu, D. Dong, Y. Sun, Y. Dai, S. Wang, H. Qian, Z. Lin, L. Chen, Cationic Covalent Organic Framework Nanosheets for Fast Li-Ion Conduction, J. Am. Chem. Soc. 140 (2018) 896–899, https://doi.org/10.1021/jacs.7b12292.

[36] L. He, S. Liu, L. Chen, X. Dai, J. Li, M. Zhang, F. Ma, C. Zhang, Z. Yang, R. Zhou, Z. Chai, S. Wang, Mechanism unravelling for ultrafast and selective (99)TcO4 (-) uptake by a radiation-resistant cationic covalent organic framework: a combined radiological experiment and molecular dynamics simulation study, Chem. Sci. 10 (2019) 4293–4305, https://doi.org/10.1039/c9sc00172g.

[37] H.-J. Da, C.-X. Yang, H.-L. Qian, X.-P. Yan, A knot-linker planarity control strategy for constructing highly crystalline cationic covalent organic frameworks: decoding the effect of crystallinity on adsorption performance, J. Mater. Chem. A 8 (2020) 12657–12664, https://doi.org/10.1039/d0ta01037e.

[38] M. Zhang, J. Chen, S. Zhang, X. Zhou, L. He, M.V. Sheridan, M. Yuan, M. Zhang, L. Chen, X. Dai, F. Ma, J. Wang, J. Hu, G. Wu, X. Kong, R. Zhou, T.E. Albrecht-Schmitt, Z. Chai, S. Wang, Electron Beam Irradiation as a General Approach for the Rapid Synthesis of Covalent Organic Frameworks under Ambient Conditions, J. Am. Chem. Soc. 142 (2020) 9169–9174, https://doi.org/10.1021/jacs.0c03941.

[39] D. Zhu, Z. Zhang, L.B. Alemany, Y. Li, N. Nnorom, M. Barnes, S. Khalil, M. M. Rahman, P.M. Ajayan, R. Verduzco, Rapid, Ambient Temperature Synthesis of Imine Covalent Organic Frameworks Catalyzed by Transition-Metal Nitrates, Chem. Mater. 28 (2021) 626–631, https://doi.org/10.1021/acs.chemmater.1c00737.

[40] M. Matsumoto, R.R. Dasari, W. Ji, C.H. Feriante, T.C. Parker, S.R. Marder, W. R. Dichtel, Rapid, Low Temperature Formation of Imine-Linked Covalent Organic Frameworks Catalyzed by Metal Triflates, J. Am. Chem. Soc. 139 (2017) 4999–5002, https://doi.org/10.1021/jacs.7b01240.

[41] W. Zhao, P. Yan, H. Yang, M. Bahri, A.M. James, H. Chen, L. Liu, B. Li, Z. Pang, R. Clowes, N.D. Browning, J.W. Ward, Y. Wu, A.I. Cooper, Using sound to synthesize covalent organic frameworks in water, Nat. Synth. 1 (2022) 87–95, https://doi.org/10.1038/s44160-021-00005-0.

[42] N. Huang, P. Wang, M.A. Addicoat, T. Heine, D. Jiang, Ionic Covalent Organic Frameworks: Design of a Charged Interface Aligned on 1D Channel Walls and Its Unusual Electrostatic Functions, Angew. Chem. Int. Ed. 56 (2017) 4982–4986, https://doi.org/10.1002/anie.201611542.

[43] P. Mo, D. Fu, P. Chen, Q. Zhang, X. Zheng, J. Hao, X. Zhuang, H. Liu, G. Liu, W. Lv, Ionic Covalent Organic Frameworks for Non-Steroidal Anti-Inflammatory Drugs (NSAIDs) Removal from Aqueous Solution: Adsorption Performance and Mechanism, Sep. Purif. Technol. 278 (2021), https://doi.org/10.1016/j.seppur.2021.119238.

[44] H. Sun, Z. Jin, C. Yang, R.L. Akkermans, S.H. Robertson, N.A. Spenley, S. Miller, S. M. Todd, COMPASS II: extended coverage for polymer and drug-like molecule databases, J. Mol. Model. 22 (2016) 47, https://doi.org/10.1007/s00894-016-2909-0.
[45] J.-X. Guo, C. Yang, X.-P. Yan, "Thiol–ene" click synthesis of chiral covalent organic frameworks for gas chromatography, J. Mater. Chem. A 9 (2021) 21151–21157, https://doi.org/10.1039/d1ta04621g.
[46] S. Kandambeth, A. Mallick, B. Lukose, M.V. Mane, T. Heine, R. Banerjee, Construction of crystalline 2D covalent organic frameworks with remarkable chemical (acid/base) stability via a combined reversible and irreversible route, J. Am. Chem. Soc. 134 (2012) 19524–19527, https://doi.org/10.1021/ja308278w.
[47] X. Guo, J. Wang, A general kinetic model for adsorption: Theoretical analysis and modeling, J. Mol. Liq. 288 (2019), https://doi.org/10.1016/j.molliq.2019.111100.
[48] Y. Cui, W. Kang, L. Qin, J. Ma, X. Liu, Y. Yang, Magnetic surface molecularly imprinted polymer for selective adsorption of quinoline from coking wastewater, Chem. Eng. J. 397 (2020), https://doi.org/10.1016/j.cej.2020.125480.
[49] Y. Zhou, Y. Hu, W. Huang, G. Cheng, C. Cui, J. Lu, A novel amphoteric β-cyclodextrin-based adsorbent for simultaneous removal of cationic/anionic dyes and bisphenol A, Chem. Eng. J. 341 (2018) 47–57, https://doi.org/10.1016/j.cej.2018.01.155.
[50] A. Farrukh, A. Akram, A. Ghaffar, S. Hanif, A. Hamid, H. Duran, B. Yameen, Design of polymer-brush-grafted magnetic nanoparticles for highly efficient water remediation, ACS Appl. Mater. Interfaces 5 (2013) 3784–3793, https://doi.org/10.1021/am400427n.
[51] S. Nayab, A. Farrukh, Z. Oluz, E. Tuncel, S.R. Tariq, H. ur Rahman, K. Kirchhoff, H. Duran, B. Yameen, Design and fabrication of branched polyamine functionalized mesoporous silica: an efficient absorbent for water remediation, ACS Appl. Mater. Interfaces 6 (2014) 4408–4417, https://doi.org/10.1021/am500123k.
[52] N. Huang, L. Zhai, H. Xu, D. Jiang, Stable Covalent Organic Frameworks for Exceptional Mercury Removal from Aqueous Solutions, J. Am. Chem. Soc. 139 (2017) 2428–2434, https://doi.org/10.1021/jacs.6b12328.
[53] H.L. Qian, M.S. Zhu, M.L. Du, X.Q. Ran, X.P. Yan, Engineering linkage as functional moiety into irreversible thiourea-linked covalent organic framework for ultrafast adsorption of Hg(II), J. Hazard. Mater. 427 (2022), 128156, https://doi.org/10.1016/j.jhazmat.2021.128156.
[54] J. Luo, X. Luo, J. Crittenden, J. Qu, Y. Bai, Y. Peng, J. Li, Removal of Antimonite (Sb(III)) and Antimonate (Sb(V)) from Aqueous Solution Using Carbon Nanofibers That Are Decorated with Zirconium Oxide (ZrO2), Environ. Sci. Technol. 49 (2015) 11115–11124, https://doi.org/10.1021/acs.est.5b02903.
[55] N. Prasetya, K. Li, MOF-808 and its hollow fibre adsorbents for efficient diclofenac removal, Chem. Eng. J. 417 (2021), https://doi.org/10.1016/j.cej.2021.129216.
[56] R. Zhao, H. Zheng, Z. Zhong, C. Zhao, Y. Sun, Y. Huang, X. Zheng, Efficient removal of diclofenac from surface water by the functionalized multilayer magnetic adsorbent: Kinetics and mechanism, Sci. Total. Environ. 760 (2021), 144307, https://doi.org/10.1016/j.scitotenv.2020.144307.
[57] W. Wang, S. Deng, D. Li, L. Ren, B. Wang, J. Huang, Y. Wang, G. Yu, Adsorptive removal of organophosphate flame retardants from water by non-ionic resins, Chem. Eng. J. 354 (2018) 105–112, https://doi.org/10.1016/j.cej.2018.08.002.
[58] R. Custelcean, B.A. Moyer, Anion Separation with Metal-Organic Frameworks, European J. Inorg. Chem. 2007 (2007) 1321–1340, https://doi.org/10.1002/ejic.200700018.
[59] D. Sheng, L. Zhu, C. Xu, C. Xiao, Y. Wang, Y. Wang, L. Chen, J. Diwu, J. Chen, Z. Chai, T.E. Albrecht-Schmitt, S. Wang, Efficient and Selective Uptake of TcO4(-) by a Cationic Metal-Organic Framework Material with Open Ag(+) Sites, Environ. Sci. Technol. 51 (2017) 3471–3479, https://doi.org/10.1021/acs.est.7b00339.
[60] Z. Jin, X. Wang, Y. Sun, Y. Ai, X. Wang, Adsorption of 4-n-Nonylphenol and Bisphenol-A on Magnetic Reduced Graphene Oxides: A Combined Experimental and Theoretical Studies, Environ. Sci. Technol. 49 (2015) 9168–9175, https://doi.org/10.1021/acs.est.5b02022.
[61] C. Chen, D. Chen, S. Xie, H. Quan, X. Luo, L. Guo, Adsorption Behaviors of Organic Micropollutants on Zirconium Metal-Organic Framework UiO-66: Analysis of Surface Interactions, ACS Appl. Mater. Interfaces 9 (2017) 41043–41054, https://doi.org/10.1021/acsami.7b13443.
[62] X. Li, Y. Qi, G. Yue, Q. Wu, Y. Li, M. Zhang, X. Guo, X. Li, L. Ma, S. Li, Solvent- and catalyst-free synthesis of an azine-linked covalent organic framework and the induced tautomerization in the adsorption of U(vi) and Hg(ii), Green Chem. 21 (2019) 649–657, https://doi.org/10.1039/c8gc03295e.
[63] H.L. Qian, F.L. Meng, C.X. Yang, X.P. Yan, Irreversible Amide-Linked Covalent Organic Framework for Selective and Ultrafast Gold Recovery, Angew. Chem. Int. Ed. 59 (2020) 17607–17613, https://doi.org/10.1002/anie.202006535.
[64] O. Buyukcakir, S.H. Je, S.N. Talapaneni, D. Kim, A. Coskun, Charged Covalent Triazine Frameworks for CO2 Capture and Conversion, ACS Appl. Mater. Interfaces 9 (2017) 7209–7216, https://doi.org/10.1021/acsami.6b16769.
[65] S.-B. Yu, H. Lyu, J. Tian, H. Wang, D.-W. Zhang, Y. Liu, Z.-T. Li, A polycationic covalent organic framework: a robust adsorbent for anionic dye pollutants, Polym. Chem. 7 (2016) 3392–3397, https://doi.org/10.1039/c6py00281a.